ISSN 0915-633X

NATIONAL INSTITUTE FOR FUSION SCIENCE

Edge Poloidal Rotation Profiles of H-mode Plasmas in the JFT-2M Tokamak

K. Ida, S. Hidekuma, M. Kojima, Y. Miura, S. Tsuji, K. Hoshino, M. Mori, N. Suzuki, T. Yamauchi and JFT-2M Group

(Received – Nov. 14, 1991)

NIFS-124 Dec. 1991

RESEARCH REPORT
NIFS Series

NAGOYA, JAPAN

Edge Poloidal Rotation Profiles of H-mode Plasmas in the JFT-2M Tokamak

K.Ida, S.Hidekuma and M.Kojima
National Institute for Fusion Science
Nagoya, 464-01, Japan

Y.Miura, S.Tsuji, K.Hoshino, M.Mori, N.Suzuki,
T.Yamauchi and JFT-2M Group
Japan Atomic Energy Research Institute
Naka-machi, Naka-gun, Ibaraki, 319-11, Japan

Parameter dependence of radial structure of edge poloidal rotation is studied with spectroscopic measurements for L- and H-mode plasmas in the JFT-2M tokamak. The peak of poloidal flow in the electron diamagnetic direction suddenly appears near the plasma edge in H-mode. No critical normalized ion collisionality, ν_{*i}, for the transition of L- to H-mode is observed. The size of the poloidal flow in H-mode has no dependence on poloidal gyro-radius.

Keywords

H-mode, Tokamak, Poloidal rotation, Radial electric field, Charge-exchange spectroscopy

1. Introduction

Since the sudden transition from low confinement (L-mode) to high confinement (H-mode) was discovered in ASDEX[1], it has been observed in many tokamaks[2-7] with several heating and operational schemes[8-11]. The H-mode transition is characterized by an improvement in both particle and energy confinement. A rapid increase in density in conjunction with a sudden drop of the H_α/D_α recycling light is a common H-mode characteristic. Recently the poloidal rotation velocity and the radial electric field near the plasma periphery have been found to play an important role in the L- to H-mode transition[12-17]. The L- to H-mode transition has been demonstrated to be triggered by driving a radial current across the outer magnetic surface[12]. The driving current and radial electric field imposed by electrodes can be positive or negative in H-mode[13]. However, without external driving current, the sudden change of edge poloidal rotation velocity is in the electron diamagnetic direction, which indicates a sudden change of radial electric field to be more negative, as was observed at L- to H-mode transitions in DIII-D[14]. The L- to H-mode transition is also associated with a sudden decrease in the edge density fluctuations and magnetic fluctuations[15,16]. This negative radial electric field is driven by some non-ambipolar fluxes such as thermal and/or fast ion loss at the plasma edge. More recently, profiles of the radial electric field at the plasma edge were measured in JFT-2M and

preliminary results were reported[17].

Theoretical models for the L- to H-mode transition have been proposed since the discovery of H-mode. Recently various models based on bipolar ion orbit loss[18-20], neoclassical viscosity[21,22], fluctuation suppression,[23] spontaneous poloidal spin-up[24], or power flow asymmetry[25] have been proposed by S.-I.Itoh, K.C.Shaing, H.Biglari, A,B,Hassam and M.Tendler to explain the sudden change of poloidal rotation velocity at the L/H transition. However, predicted features of poloidal rotation velocity and the radial electric field are different among models. It is therefore crucial to study precise profiles of poloidal flow and parameter dependence of poloidal rotation and the radial electric field at L to H transitions. In this paper we present more details of previous results[17], and comparison with several current theories is also discussed.

2. Measurements of poloidal flow and radial electric field

The radial electric field profiles are inferred from poloidal/toroidal rotation and ion pressure profiles using the ion momentum balance equation;

$$E_r = \frac{\partial p_i}{eZ_i n_i \partial r} - (B_\theta V_\varphi - B_\varphi V_\theta),$$

where Z_i, p_i, n_i are the ion charge, pressure and density, B_φ and B_θ are the toroidal and poloidal magnetic fields, and v_φ and v_θ are the toroidal and poloidal rotation velocities. Toroidal rotation velocity is in the same order of poloidal rotation velocity at the plasma edge. The contribution of toroidal rotation velocity to the electric field is much smaller than that of poloidal rotation velocity, since the poloidal magnetic field is smaller than the toroidal magnetic field by one order of magnitude. The dominant impurity in JFT-2M is carbon and its amount is estimated from the intensity of CVI emission. The radial electric field is estimated using the momentum balance equation of carbon, since there is no guarantee that bulk ions rotate with the same velocity as carbon when the plasma changes quickly at L/H transition[26].

The toroidal rotation velocity, ion temperature and fully stripped carbon density profiles are measured using the charge exchange spectroscopy technique at CVI 5292 Å with toroidal arrays (two sets of 34 channels) with a spatial resolution of 1 cm. The poloidal rotation and edge ion temperature profiles are measured using the intrinsic radiation of CVI at 5292 Å. The two sets of toroidal/poloidal arrays view the plasma in opposite directions to define the zero reference for Doppler shift measurements.The poloidal arrays (two set of 23 channels) do not view across the beam line and view only the plasma periphery with a spatial resolution of 4 mm. The integration effect of

line-of-sight in poloidal arrays is small, as long as the signal increases rapidly with smaller minor plasma, even though the emission shell extends well inside the plasma. However in order to avoid the integration problem of line-of-sight completely, an wavelength-resolved Abel inversion[27] is used to obtain local ion temperature and poloidal rotation velocity from the poloidal arrays.

The optical fibers (114 channels) are led to the entrance slit of a 1 m Czerny-Tunner spectrometer with 2160/mm grating and the entrance slit is effectively divided by the 114 channels in height. The effective slit width is determined by the number of fiber lines. Since the diameter of each fiber is 0.125 mm, the effective slit width can be varied 0.25 or 0.5 mm. The slit width for poloidal and edge toroidal channels is 0.25 mm, while it is 0.5 mm for the central toroidal channels that are viewing the high ion temperature region of the plasma. A CCD detector is coupled with an image intensifier (micro channel plate) by an image fiber bundle and is arranged at the exit plane. An extensive spatial calibration of the 114 channels has been done with a mercury pen lamp set on the vacuum vessel using calibration optical fibers set into the toroidal/poloidal arrays. The location of the spot from the mercury lamp on the CCD detector was measured and this data has been used for the position calibration. The uncertainty in position is less than 5 mm, which has been confirmed by the fact that the position of the sharp edge of CVI emission from the toroidal arrays agrees

with that measured in the poloidal arrays. The uncertainty of the position of the separatrix calculated with an equilibrium code is also estimated to be 5 mm. The fine-structure components due to different l-level states increases the apparent Doppler width in the measurements of the low ion temperature plasma. However, the increase of apparent ion temperature from real temperature is 15 % at 100 eV for the n=8-7 transition[28]. The correction due to fine-structure is taken into account in our analysis, however it is a minor correction compared with the uncertainty in the fitting the measured spectrum.

The electron temperature profile and its gradient profile are measured with an ECE radiometer to investigate the location of the thermal transport barrier. The plasma near the periphery ($r/a > 0.9$) is not optically thick for emission at the second harmonic of the electron cyclotron frequency. The ECE temperature at this location is not accurate unless the emission is reflected at the wall making the plasma effectively more optically thick. The reflection coefficient determined from the intensity ratio of second to third harmonic ECE signal is 0.88 in JFT-2M[28]. The electron temperature at the plasma edge is found to be underestimated by 20-30%. The spatial resolution of the measurements, set by the frequency bandwidth of the detector, is 3 mm. Bulk electron density (n_e) and temperature (T_e) are measured with Thomson scattering. The edge plasma space potential profiles are derived from T_e and floating potential measurements from a Langmuir probe outside of the separatrix.

3. Radial structure of poloidal flow and radial electric field

Figure 1 shows the time evolution of the poloidal rotation velocity for a hydrogen plasma with a current of 280 kA, a toroidal field of 1.3 T, q_ψ of 2.7, a major radius of 1.3 m and a minor radius of 0.3 m in a single null divertor configuration. The neutral beam is injected at 700 ms in the co-direction with a power of 0.7 MW and another beam is injected at 730 ms in the counter direction with a power of 0.3 MW to exceed the power threshold for L/H transition at 760 ms. A jump of poloidal rotation velocity at the L/H transition is observed at 1.3 cm and 0.3 cm inside the separatrix and 0.2 cm outside the separatrix, while no jump of poloidal rotation velocity is observed 2.2 cm inside and 0.7 cm outside the separatrix. The poloidal rotation increases in the electron diamagnetic direction in the H-mode regardless of the direction of plasma current and neutral beam injection. The change of poloidal rotation is prior to the change of ion temperature and is fairly localized near the separatrix, while the sharp gradient in the ion temperature is observed further inside the separatrix as shown in Figure 2. The ion temperature at ds = -2.2 cm increases significantly 50 ms after the L/H transition. However, in H-mode with ELMs, no poloidal rotation velocity shear is observed, even though a steep gradient in ion temperature is observed. This is mainly due to the poor time resolution of the measurements. The fast change of poloidal rotation can be easily masked, since the

change of Doppler shifts within the integration period produces effective Doppler broadening. This broadening due to the rapid shift of central wavelength during integration increase the apparent ion temperature by 20-30% in our experimental condition.

The profiles of ion/electron temperature before (t = 708, 742 ms) and after (t= 775, 808 ms) the L/H transition are shown in Figure 3. Both electron and ion temperature profiles show a clear pedestal at averaged minor radius of 0.9 during the H-mode phase. The increase of electron temperature is simply due to the improvement of electron thermal transport. However the increase of central ion temperature in the H-mode phase is due to both the improvement of ion energy transport and the increase of power flow from electrons at higher electron density. The electric field profiles for ohmic, L-mode and H-mode plasmas are calculated from rotation velocities and pressure gradients of carbon using a momentum balance equation of C^{5+} [eq. 1]. The electric field becomes more negative in H-mode, due to an increase of poloidal rotation in the electron diamagnetic direction. The poloidal rotation velocity profiles and ion temperature profiles at ohmic (t = 692 ms), L-mode (t = 742 ms) and H-mode (t = 792 ms) are shown in Figure 4. The plasma always rotates in the ion diamagnetic direction outside the separatrix and in the electron diamagnetic direction inside the separatrix. The structure of poloidal flow is consistent with the measurements of phase velocity of the turbulent fluctuations in

TEXT tokamak[30]. The position, where the plasma does not rotate poloidally, moves outward as the plasma changes from ohmic to L- and the H-mode. These structure of poloidal flow imply that the poloidal flow is convective as the M.Tendler model predicts.

The gradient of the electric field inside the separatrix, ds = -1.5 cm, is positive in ohmic phase, slightly positive in L-mode and becomes negative in the H-mode. The relative space potentials in the plasma are derived by integrating the radial electric field. Combining the measurements of space potential with electric probes, the profiles of space potential for ohmic, L-mode and H-mode are obtained as shown in Fig.5(b). The space potentials just inside the separatrix are positive in ohmic and L-mode and negative in H-mode. This negative space potential is -260 V, while the ion temperature is 170 eV at the thermal barrier. These measurements indicate that the improvement of thermal transport correlates to the negative $\partial E_r/\partial r$. In conclusion, both E_r and $\partial E_r/\partial r$ become more negative in the thermal barrier, 1-2 cm inside the separatrix, after the L/H transition. Positive $\partial E_r/\partial r$ is observed outside of the separatrix both for L- and H-mode plasmas.

4. Velocity shear and thermal barrier

The ion thermal transport barrier is always found at 1-2 cm inside the separatrix although the steep gradients of electron density and the brightness of CVI emission is concentrated near

the plasma edge within 0.5 cm of the separatrix. Figure 6 shows the gradient of electron and ion temperature as a function of poloidal rotation velocity shear 1.5 cm inside the separatrix for various discharges. Poloidal rotation shear is positive or a little negative $\partial v_\theta/\partial r > -2$ kms^{-1}cm^{-1}, with small gradients of electron and ion temperature, $\partial T_e/\partial r < 40$ eV/cm and $\partial T_i/\partial r < 20$ eV/cm, for L-mode plasma. On the other hand, the poloidal rotation shear is always negative during large gradients of electron and ion temperature, 40 eV/cm $< \partial T_e/\partial r <$ 90 eV/cm, 20 eV/cm $< \partial T_i/\partial r <$ 70 eV/cm, in H-mode plasma. Both the electron temperature gradient and poloidal rotation velocity shear become larger as the plasma current of the discharge is increased from 170 kA to 280 kA.

The large electron temperature gradient is associated with negative poloidal rotation velocity shear not positive rotation shear. This sign dependence of poloidal rotation shear on improvement of heat transport is one of the important characteristics in the L/H transition of the plasma with no externally driven electric field. The ion temperature gradients show similar behavior, but the gradients of ion temperature are slightly smaller than the electron temperature gradient. This is consistent in that most of the heating power of the neutral beam is into electrons, so at the plasma edge low temperature ions are heated through collision with electrons.

Bulk ion temperature and rotation velocity are assumed to be the same as carbon temperature and rotation velocity. In order to obtain a wide range of ion normalized collisionality,

poloidal rotation velocities are measured for H-mode discharges with various electron densities and plasma currents. The poloidal rotation parameter $U_p(=v_\theta B/v_{th}B_\theta)$ is plotted as a function of normalized ion collisionality in Figure 7. The ion collisionality ν_{*i} at 0.7 cm inside the separatrix is obtained with the edge ion temperature measured with CVI line and the edge electron density extrapolated from FIR interferometer measurements. The extrapolated edge densities are consistent with the probe measurements. The ion collisionality ν_{*i} decreases after the L/H transition for the discharges with higher plasma current, while it increases or does not change for lower plasma current. This is mainly due to the fact that the ion temperature increases more than the electron density for higher current, but increases less than the electron density for lower current.The poloidal rotation parameter charges from below two to above two at L to H transitions. Although there is no critical ion collisionality for the L/H transition, critical values of the poloidal rotation parameter is observed. This critical poloidal rotation parameter, U_p, at the L/H transition is 2 - 3 across a wide range of ion normalized collisionality.

Figure 8 shows the width of the poloidal rotation shear for various poloidal gyro-radius width with plasma current of 170 kA to 280 kA and with hydrogen and deuterium working gas. The widths of poloidal rotation velocity, $L(v_\theta)$, are defined by the two times of the full width of half maximum (2 x FWHM) of poloidal rotation velocity in H-mode. They are ~4 cm over a

wide range of poloidal gyro-radius from 0.7 cm to 2 cm. The width of the poloidal rotation velocity shear is two to six poloidal gyro-radius, however it shows no dependence on gyro-radius.

5. Discussions

Since several H-mode models have been proposed, we now discuss the agreements and discrepancies of each model to our observations. Comparison of characteristic parameters in H-mode plasma between JFT-2M measurements and theories is summarized in Table I. The L/H transition compared here is only spontaneous transition during plasma heating. These transitions must have features different from the L/H transitions triggered by driving a radial current across the outer magnetic surface[12,13]. The radial electric field inside the separatrix is negative in the spontaneous H-mode as observed in JFT-2M, although it can be negative or positive when the driving current is induced and radial electric filed is imposed externally[13].

In Itoh's model, non-ambipolar particle losses determine the self consistent radial electric field with positive values of $\partial E_r/\partial r$ in L-mode and negative values of $\partial E_r/\partial r$ in H-mode being predicted. This negative $\partial E_r/\partial r$ is also predicted to reduce the banana width of ions and the electron anomalous flux by improved micro-stability[18-20]. It also is interesting to evaluate the strength of the gradient of the radial electric field $\partial E_r/\partial r$,

since it can affect the ion orbit and change the banana width of ions by the factor of $(|1-u_g|+C\varepsilon)^{-1/2}$, where ε and C are the inverse aspect ratio and a numerical coefficient. The shear parameter of the electric field u_g, defined by $\rho_p(\partial E_r/\partial r)/v_{th}B_\theta$, is in the range of $-0.5 < u_g < 1$ for L-mode and $-2 < u_g < -0.5$ for H-mode at 0.7 cm inside the separatrix. The gradient of the electric field measured in H-mode is large enough to change the banana width. These values of the shear parameter u_g is consistent with the prediction of Itoh's model, 1.0 in L-mode and -2.3 in H-mode[20]. The pressure gradient parameter, λ [$-(T_e/T_i)\rho_p \{(\partial n_e/\partial r)/n_e+\alpha(\partial T_e/\partial r)/T_e)\}$] defined in their model, changes from below unity ~ 0.5 to above unity ~ 1.3, at L/H transition and is consistent with the critical value of their model ($\lambda_c \approx 1$). We observe qualitative agreement of characteristic parameters u_g and λ_c in Itoh's model at the L/H transition. However the lack of dependence of the width of the sheared flow region on poloidal gyro-radius contradicts their model.

On the other hand, in K.C.Shaing's model[21], the bifurcation of poloidal viscosity at the critical normalized ion collisionality play a more important role than the sign of $\partial E_r/\partial r$ at the L/H transition. The corresponding negative radial electric filed E_r suppresses the fluctuations[22]. These critical rotation values agree with the prediction of Shaing's model (U_p ~ 1 for L-mode and 2 for H-mode) within a factor of two. The collisionality parameter of Shaing's model for the L/H

transition varies with machine geometry and the fraction of fast ion loss. His model predicts a critical value of ν_{*i} (1 ~ 2) at L/H transition, which does not agree with the measurements. The effect of fast ion loss, which is not included in his model, may increase the critical value of ν_{*i}, since the fast ion loss produces an effective radial current. The large value of critical ν_{*i} measured in JFT-2M may be explained with Shaing's model by including the additional effect of fast ion loss[31]. Models which include fast ion loss as well as bulk ions are necessary to have better agreement with the experimental observations. We observe qualitative agreement of characteristic parameters U_p in K.C.Shaing's model[21] at the L/H transition. The Shaing's model explains that the suppression of fluctuations are due to the more negative electric field not positive E_r[22], which is consistent with the dependence of temperature gradients on the sign of poloidal rotation and radial electric field observed in JFT-2M. His model also predicts a poloidal gyro-radius dependence of the width of poloidal rotation shear as well as Itoh's model, since ion orbit losses are the driving force of poloidal rotation. Recently, the complete effect of the orbit squeezing are studied and it is found theoretically that the width of the edge radial electric field layer in the H-mode as estimated from the ion orbit loss model does not depend explicitly on the poloidal gyro-radius[32].

The influence of sheared poloidal rotation has been investigated by H.Biglari, and turbulence is expected to be suppressed by either sign of radial electric shear[23]. However

clear sign dependence of improvement of thermal transport on $\partial E_r/\partial r$ and $\partial v_\theta/\partial r$ is observed. The L to H transition is observed only when the velocity shear becomes negative not when the velocity shear is positive. There is no critical $|\partial v_\theta/\partial r|$ for L/H transition. Improvement of transport and suppression of turbulence due to sheared flow is an important mechanism associated with the L- to H-mode transition, however there is no experimental evidence to support that the sheared flow causes the L/H transition. Although Biglari theory predicts that both negative ($\partial E_r/\partial r < 0$) and positive ($\partial E_r/\partial r > 0$) electric field shear can suppress the fluctuations, however, negative shear is more beneficial to the the improvement of thermal transport in experiment.

A.B.Hassam proposed a mechanism for poloidal spin-up that does not rely on non-ambipolar flux such as edge ion loss and does not depend on the ion collisionality parameter and poloidal gyro-radius[24]. In his model, when the poloidal asymmetry, the fractional difference between the particle transport inside and outside, is sufficiently large, and the particle transport rate is larger than the damping due to magnetic pumping, poloidal spin-up occurs. This spin-up is characterized by simultaneous sudden changes in both poloidal and toroidal flow velocity, which has not been observed at least JFT-2M H-mode. None of these models can fully explain the structure of edge electric field, negative $\partial E_r/\partial r$ inside and positive $\partial E_r/\partial r$ outside the separatrix, since they solve problems only inside the

separatrix.

M.Tendler's model deals with the problem both inside and outside the separatrix, in the scrape-off layer (SOL)[25]. His model predicts that the direction of the poloidal rotation in the SOL is opposite to the direction of the neoclassical poloidal rotation on the inner flux surface just inside the separatrix. These two opposite flows are consistent with the measurements in JFT-2M. In order to compare the measurements with this model, measurements of the 2D poloidal flow pattern in the vicinity of the separatrix is necessary.

In conclusion, two opposite poloidal flows are observed in the vicinity of the separatrix. Flow is in the electron diamagnetic direction inside and ion diamagnetic direction outside the separatrix. The poloidal flow inside increases in magnitude and has a peak close to the separatrix in H-mode. The thermal barrier, which is indicated by a large gradient of both electron and ion temperature, is only associated with a negative electric field shear ($\partial E_r/\partial r < 0$). These features are consistent with most H-mode models, however no dependence of the width of the sheared poloidal flow on poloidal gyro-radius is observed and thus contradicts the predictions of H-mode theories related to ion orbit loss. These theories must include other non-ambipolar losses such as fast ion loss.

The authors would like to thank S.-I.Itoh, K.Itoh (National Institute for Fusion Science, NIFS) and K.C.Shaing (Oak Ridge National Laboratory) and A.Leonard (General Atomics) for their

useful discussions. The authors also thank the support of data acquisition by T.Matsuda (Japan Atomic Energy Research Institute, JAERI), the support of diagnostic by T.Yamauchi, H.Tamai, H.Ogawa (JAERI), and the support by tokamak and NBI operation staff in JFT-2M. Continuous encouragement by H.Maeda (JAERI), Y.Hamada(NIFS), K.Matsuoka (NIFS) is acknowledged.

References

[1]F.Wagner G.Becker, K.Behringer, D.Campbell, A.Eberhangen, W.Engelhardt, G.Fussmann, O,Gehre, J.Gernhardt, G.v.Gierke, G.Haas, M.Huang, F.Karger, M.keilhacker, O.Kluber, M.Kornherr, K.Lackner, G.Lisitano, G.G.Lister, H.M.Mayer, D.Meisel, E.R.Muller, H.Murmann, H.Niedermeyer, W.Poschenrieder, H.Rapp, H.Rohr, F.Schneider, G.Siller, E.Speth, A.Stabler, K.H.Steuer, G.Venus, and O.Vollmer, Phys. Rev. Lett. **49**, 1408 (1982).

[2]S.M.Kaye M.G.Bell, K.Bol, D.Boyd, K.Brau, D.Buchenauer, R.Budny, A.Cavallo, P.Couture, T.Crowley, D.S.Darrow, H.Eubank, R.J.Fonck, R.Goldston, B.Grek, K.P.Jaehnig, D.Johnson, R.Kaita, H.Kugel, B.LeBlanc, J.Manicam, D.Manos, D.Mansfield, E.Mazzucato, R.McCann, D.McCune, K.McGuire, D.Mueller, A.Murdock, M.Okabayashi, K.Okano, D.K.Owens, D.E.Post, M.Reusch, G.L.Schmidt, S.Sesnic, R.Slusher, S.Suckewer, C.Surko, H.Takahashi, F.Tenney, H.Towner, and J.Valley, J. Nucl. Mater **121**, 115 (1984).

[3]M.Nagami, M.Kasai, A.Kitsunezaki, T.Kobayashi, S.Konoshima,

T.Matsuda, M.Miya, H.Ninomiya, S.Sengoku, M.Shimada, H.Yokomizo, T.Anmgel, C.Armentrout, F.Blau, G.Bramson, N.Brooks, R.Chase, A.Colleraine, E.Fairbanks, J.Fasolo, R.Fisher, R.Groebner, T.Hino, R.Hong, G.Jahns, J.Kamperschroer, J.Kim, A.Lieber, J.Lohr, D.McColl, L.Rottler, R.Seraydarian, R.Silagi, J.Smith, R.Snider, T.Taylor, J.Tooker, D.Vaslow, and S.Wojtowicz, Nucl. Fusion **24**, 183 (1984).

[4]A.Tanga, K.H.Behringer, A.E.Costley, M.Brusati, B.Denne, A.Edwards, A.Gibson, R.D.Gill, N.Gottardi, R.Granetz, P.J.Harbour, H.Jackel, M.Keilhacker, E.Lazzaro, M.Malacarne, P.D.Morgan, P.Noll, J.Orourke, P.E.Stott, D.R.Summers, J.A.Tagle, and P.R.Thomas, Nucl. Fusion 27, 1877 (1987).

[5]S.Sengoku, A.Finahashi, M.Hasegawa, K.Hoshino, S.Kasai, T.Kawakami, H.Kawashima, T.Matoba, T.Matsuda, H.Matsumoto, Y.Miura, M.Mori, H.Ogawa, T.Ogawa, H.Ohtsuka, T.Shoji, N.Suzuki, H.Tamai, Y.Uesugi, T.Yamamoto, and T.Yamauchi, Phys. Rev. Lett. **59,** 450 (1987).

[6]K.Toi, K.Kawahata, S.Morita, T.Watari, R.Kumazawa, K.Ida, A.Ando, Y.Oka, M.Sakamoto, Y.Hamada, K.Adati, R.Ando, T.Aoki, S.Hidekuma, S.Hirokura, O.Kaneko, A.Karita, T.Kawamoto, Y.Kawasumi, T.Kurota, K.Masai, K.Narihara, Y.Ogawa, K.Ohkubo, S.Okajima, T.Ozaki, M.Sasao, K.N.Sato, T.Seki, F.Shimpo, H.Takahashi, S.Tanahashi, Y.Taniguchi, and T.Tsuzuki, Phys. Rev. Lett. **64,** 1895 (1990).

[7]C.E.Bush, R.J.Goldston, S.D.Scott, E.D.Fredrickson, K.McGuire, J.Schivell, G.Taylor, Cris W. Barnes, M.G.Bell, R.L.Boivin,

N.Bretz, R.V.Budny, A.Cavallo, P.C.Efthimion, B.Grek, R.Hawryluk, K.Hill, R.A.Hulse, A.Janos, D.W.Johnson, S.Kilpatrick, D.M.Manos, D.K.Mansfield, D.M.Meade, H.Park, A.T.Ramsey, B.Stratton, E.J.Synakowski, H.H.Towner, R.M.Wieland, M.C.Zarnstorff, and S.Zweben, Phys. Rev. Lett. **65,** 424 (1990).

[8]K.Hoshino, T.Yamamoto, H.Kawashima, N.Suzuki, Y.Uesugi, M.Mori, H.Aikawa, S.Kasai, T.Kawakami, T.Matsuda, Y.Miura, K.Odajima, H.Ogawa, T.Ogawa, H.Ohtsuka, T.Shoji, H.Tamai, T.Yamauchi, T.Kondo, I.Nakazawa, C.R.Neufeld, and H.Maeda, Phys. Rev. Lett. **63,** 770 (1989).

[9]S.Tsuji, K.Ushigusa, Y.Ikeda, T.Imai, T.Itami, M.Nemoto, K.Nagashima, Y.Koida, Y.Kawano, T.Fukuda, T.Kondoh, M.Shimada, H.Nakamura, O.Naito, H.Yoshida, T.Nishitani, H.Kubo, K.Tobita, Y.Kusama, S.Ishida, M.Sato, N.Isei, T.Sugie, N.Miya, R.Yoshino, and K.Uehara, Phys. Rev. Lett. **64,** 1023 (1990).

[10]T.H.Osborne, N.H.Brooks, K.H.Burrell, T.N.Carlstrom, R.J.Groebner, W.Howl, A.G.Kellman, L.L.Lao, T.S.Taylor, D.N.Hill, N.Ohyabu, and M.E.Perry, Nucl. Fusion **30,** 2023 (1990).

[11]B.J.D.Tubbing, B.Balet, D.V.Bartlett, C.D.Challis, S.Corti, R.D.Gill, C.Gormezano, C.W.Gowers, M.von Hellermann, M.Hugon, J.J.Jacquinot, H.Jaeckel, P.Kupschus, K.Lawson, H.Morsi, J.O'rourke, D.Pasini, F.G.Rimini, G.Sadler, G.L.Schmidt, D.F.H,Start, P.M.Stubberfield, A.Tanga, F.Tibone, Nucl. Fusion **31,** 839 (1991).

[12]R.J.Taylor, M.L.Brown, B.D.Fried, H.Grote, J.R.Liberati, G.J.Morales, P.Pribyl, D.Darrow, and M.Ono, Phys. Rev. Lett. **63,**

2365 (1989).

[13]R.R.Weynants, and R.J.Taylor, Nucl. Fusion **30,** 945 (1990).

[14]R.J.Groebner, K.H.Burrell, and R.P.Seraydarian, Phys. Rev. Lett. **64,** 3015 (1990).

[15]K.H.Burrell, T.N.Carlstrom, E.J.Doyle, P.Gohil, R.J.Groebner, T.Lehecka, N.C.Luhmann, Jr., H.Matsumoto, T.H.Osbone, W.A.Peebles, and R.Philipona, Phys. Fluids B **2**, 1405 (1990).

[16]E.J.Doyle, R.J.Groebner, K.H.Burrell, P.Gohil, T.Lehecka, N.C.Luhmann, Jr., H.Matsumoto, T.H.Osborne, W.A.Peebles, and R.Philipona, Phys. Fluids B **3,** (1991) 2300.

[17]K.Ida, S.Hidekuma, Y.Miura, T.Fujita, M.Mori, K.Hoshino, N.Suzuki, T.Yamauchi, Phys. Rev. Lett. **65,** 1364 (1990).

[18]S.-I.Itoh and K.Itoh, Phys. Rev. Lett. **60,** 2276 (1988).

[19]S.-I.Itoh and K.Itoh, Nucl. Fusion **29,** 1031 (1989).

[20]S.-I.Itoh and K.Itoh, J. Phy. Soc. Jpn. **59,** 3815 (1990).

[21]K.C.Shaing and E.C.Crume,Jr, Phys. Rev. Lett. **63,** 2369 (1989).

[22]K.C.Shaing, E.C.Crume,Jr, and W.A.Houlberg, Phys. Fluids B **2,** 1492 (1990).

[23]H.Biglari, P.H.Diamond, and P.W.Terry, Phys. Fluids B **2,** 1 (1990).

[24]A.B.Hassam, T.M.Antonsen,Jr, J.F.Drake, and C.S.Liu, Phys. Rev. Lett. **66,** 309 (1991).

[25]M.Tendler and V.Rozhansky, Comments Plasma Phys. Controlled Fusion **13** 191 (1990).

[26]Y.B.Kim, P.H.Diamond, and R.J.Groebner, Phys. Fluids B **3,** 2050 (1991).

[27]K.Ida and S.Hidekuma, Rev. Sci. Instrum. **60,** 867 (1989).

[28]R.J.Fonck, D.S.Darrow, and K.P.Jaehnig, Phys. Rev. A **29**, 3288 (1984).

[29]K.Hoshino et al., J. Phys.Soc. Jpn. **58** 1248 (1989).

[30]Ch.P.Ritz, R.D.Bengtson, S.J.Levinson, E.J.Powers, Phys. Fluids **27** 2965 (1984).

[31]K.C.Shaing (private communication)

[32]K.C.Shaing (private communication)

Table and figure captions

Table I. Comparison of characteristic parameters in H-mode plasma between measurements and theories.

Fig.1 Time evolution of poloidal rotation velocity at (a) -0.3, -1.3 and -2.2 cm inside and (b) 0.2, 0.7 and 1.3 cm outside the separatrix. The L to H and H to L transitions occur at t = 760 and 840 ms.

Fig.2 Time evolution of the ion temperature at (a) -0.3, -1.3 and -2.2 cm inside and (b) 0.2, 0.7 and 1.3 cm outside the separatrix. The L to H and H to L transition occur at t = 760 and 840 ms. Time evolution of the electron temperature measured with ECE is also shown in Fig.(a)

Fig.3 Radial profiles of (a) electron temperature measured with ECE radiometer and (b) ion temperature measured with toroidal arrays at t = 708 and 742 ms (before the L/H transition) and t = 775 and 808 ms (after the L/H transition).

Fig.4 (a) Edge poloidal rotation velocity and (b) ion temperature as a function of the distance from the separatrix, for OH (t =692 ms, asterisk), for L-mode (t = 742 ms, open circles) and H-mode (t = 792 ms, closed symbols), where ds is negative for inside and positive for outside of the separatrix.

Fig.5 (a) Edge radial electric field and (b) space potential as a function of the distance from the separatrix, for OH (t = 692 ms, asterisk) L-mode (t = 742 ms, open symbols) and H-mode (t = 792 ms, closed symbols). The absolute value of the space potential is measured by probes (squares symbols).

Fig.6 Gradients of (a) electron temperature measured with ECE radiometer and (b) ion temperature 1.5 cm inside the separatrix as a function of poloidal rotation velocity shear. Open symbols stand for L-mode and closed symbol for H-mode. Circles are discharges with the plasma current of 280 kA and triangles are with 170 kA. Squares stand for limiter discharges with plasma current of 230 kA.

Fig.7 Normalized poloidal rotation velocity as a function of normalized ion collisionality. Open symbols stand for L-mode and closed symbols for H-mode. Circles are discharges with a plasma current of 280 kA and triangles are with 170 kA. Squares stand for a limiter discharges with plasma current of 230 kA.

Fig.8 The width of the poloidal rotation velocity shear as a function of poloidal gyro-radius Open circles are for hydrogen plasma and closed circles are deuterium plasma.

parameters	Exp.	Itoh	Shaing	Biglari	Hassam	Tendler
E_r	negative (no induced current)	positive (negative, if $\partial E_r/\partial r<0$)	negative	not important		negative
$\partial E_r/\partial r$	negative	negative	positive	positive or negative		
E_r in SOL	positive					positive
critical pressure gradient λ	~ 1	~ 1			critical density gradient	
critical $\nu*i$	none	none	1 ~ 2 if no fast ion loss	none	none	
critical $\lvert\partial v_\theta/\partial r\rvert$	none	none	none	necessity	none	
electric field shear u_g	> -0.5 ~ 0 (L) < -0.5 ~ 0 (H)	1.0 (L) -2.3 (H)				
poloidal velocity Up	< 2 ~ 3 (L) > 2 ~ 3 (H)		1 (L) 3 (H)			
dependence of shear region on poloidal gyro-radius	no	yes	yes (no, if orbit is squeezed)	no	no	

Table I

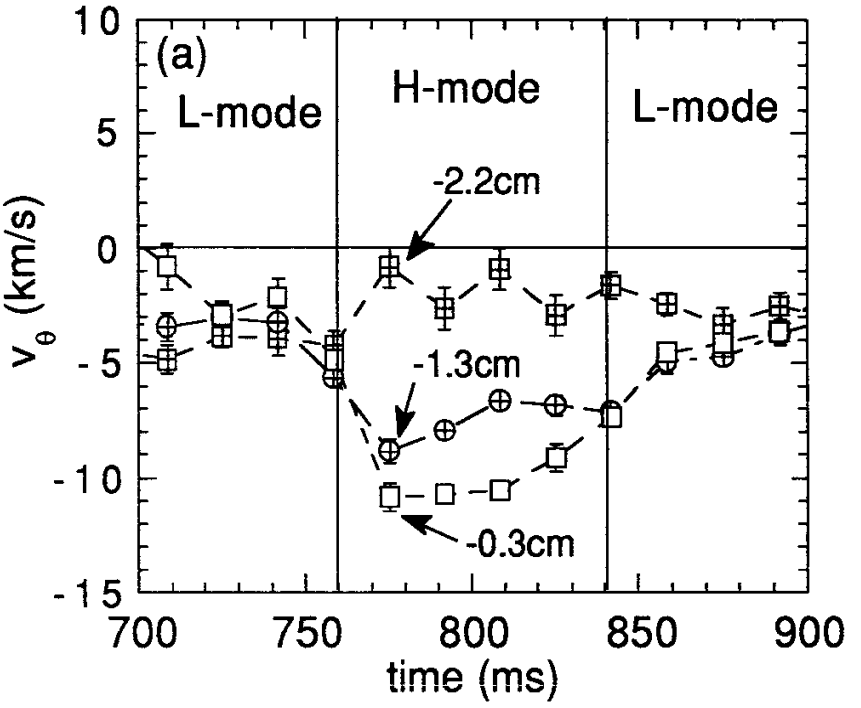
(a)
L-mode
H-mode
L-mode
-2.2cm
-1.3cm
-0.3cm
v_θ (km/s)
time (ms)
10
5
0
- 5
- 10
- 15
700
750
800
850
900

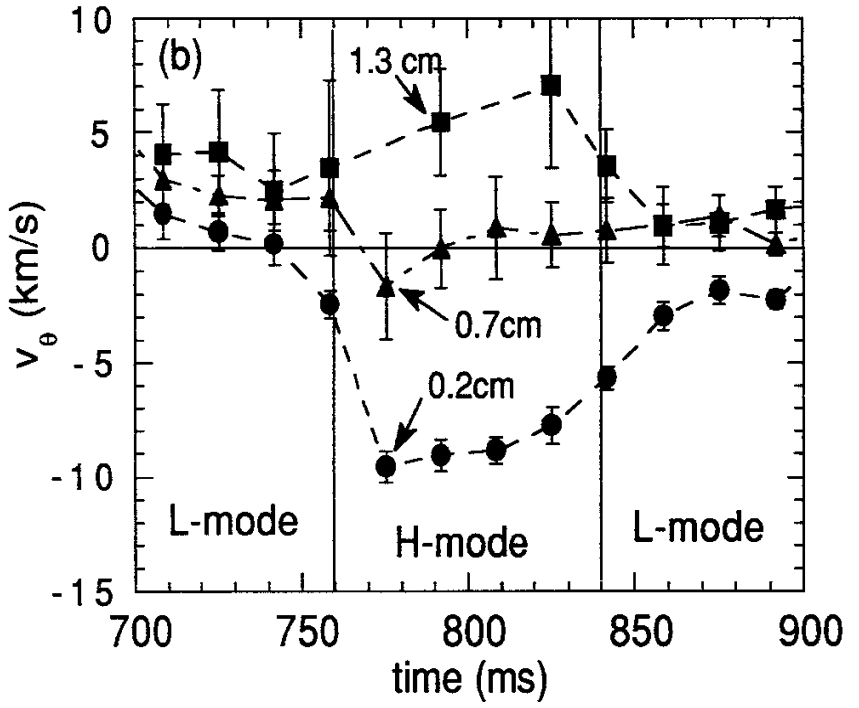
(b)
1.3 cm
0.7cm
0.2cm
L-mode
H-mode
L-mode
v_θ (km/s)
time (ms)
10
5
0
- 5
- 10
- 15
700
750
800
850
900

Figure 1

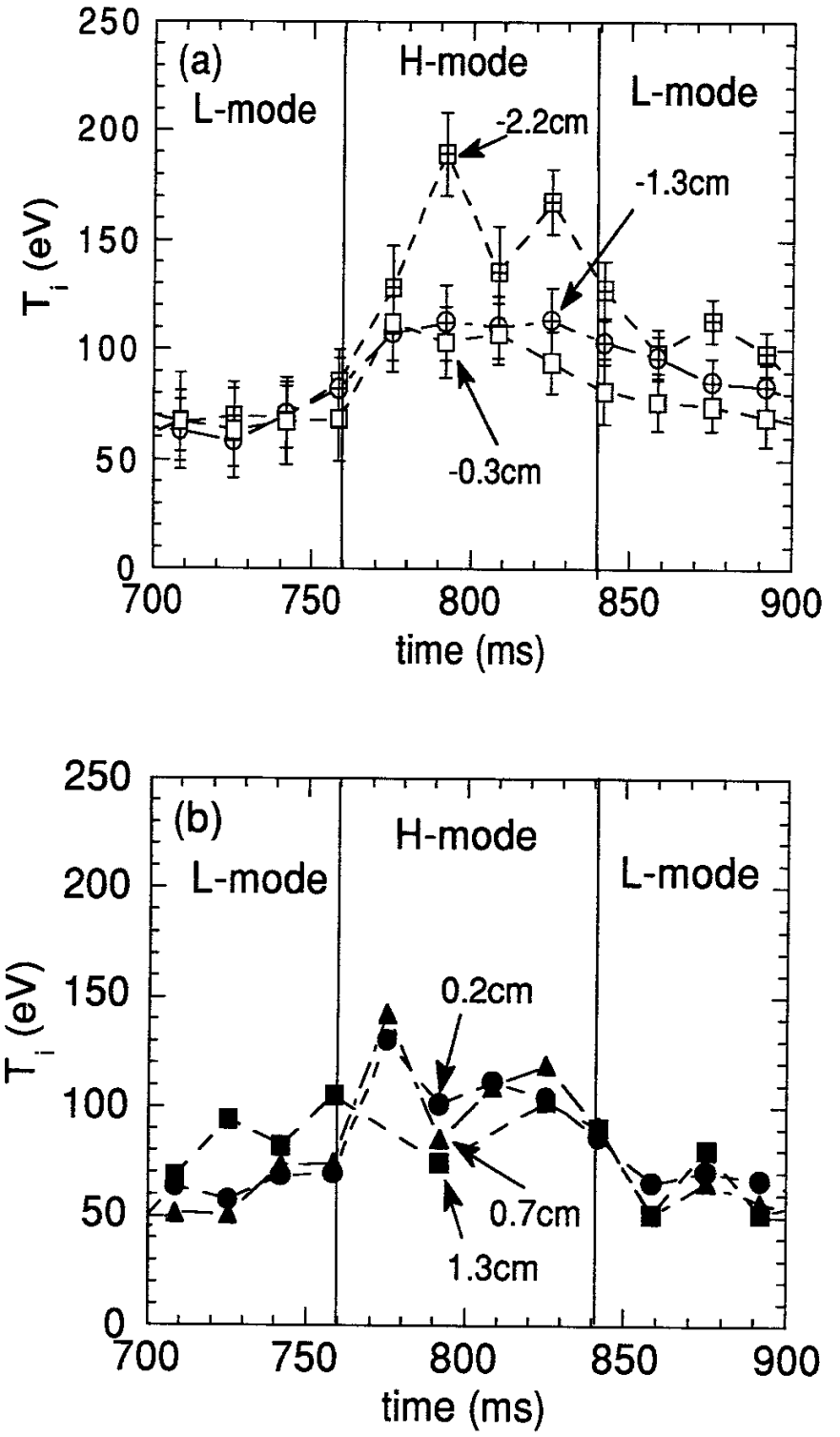
(a)
L-mode
H-mode
L-mode
-2.2cm
-1.3cm
-0.3cm
T_i (eV)
time (ms)
(b)
L-mode
H-mode
L-mode
0.2cm
0.7cm
1.3cm
T_i (eV)
time (ms)

Figure 2

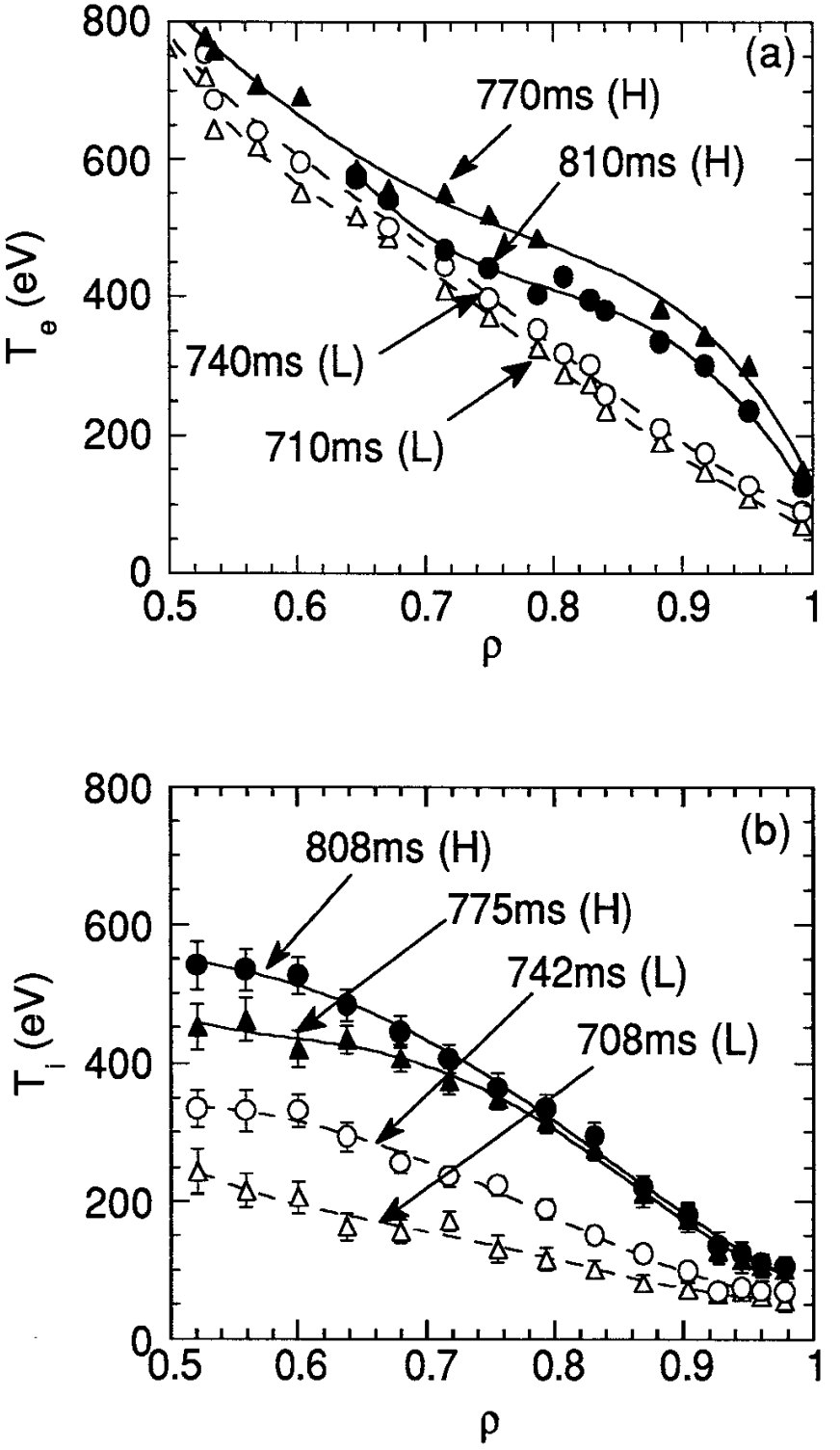
(a)
770ms (H)
810ms (H)
740ms (L)
710ms (L)
T_e (eV)
ρ
(b)
808ms (H)
775ms (H)
742ms (L)
708ms (L)
T_i (eV)
ρ

Figure 3

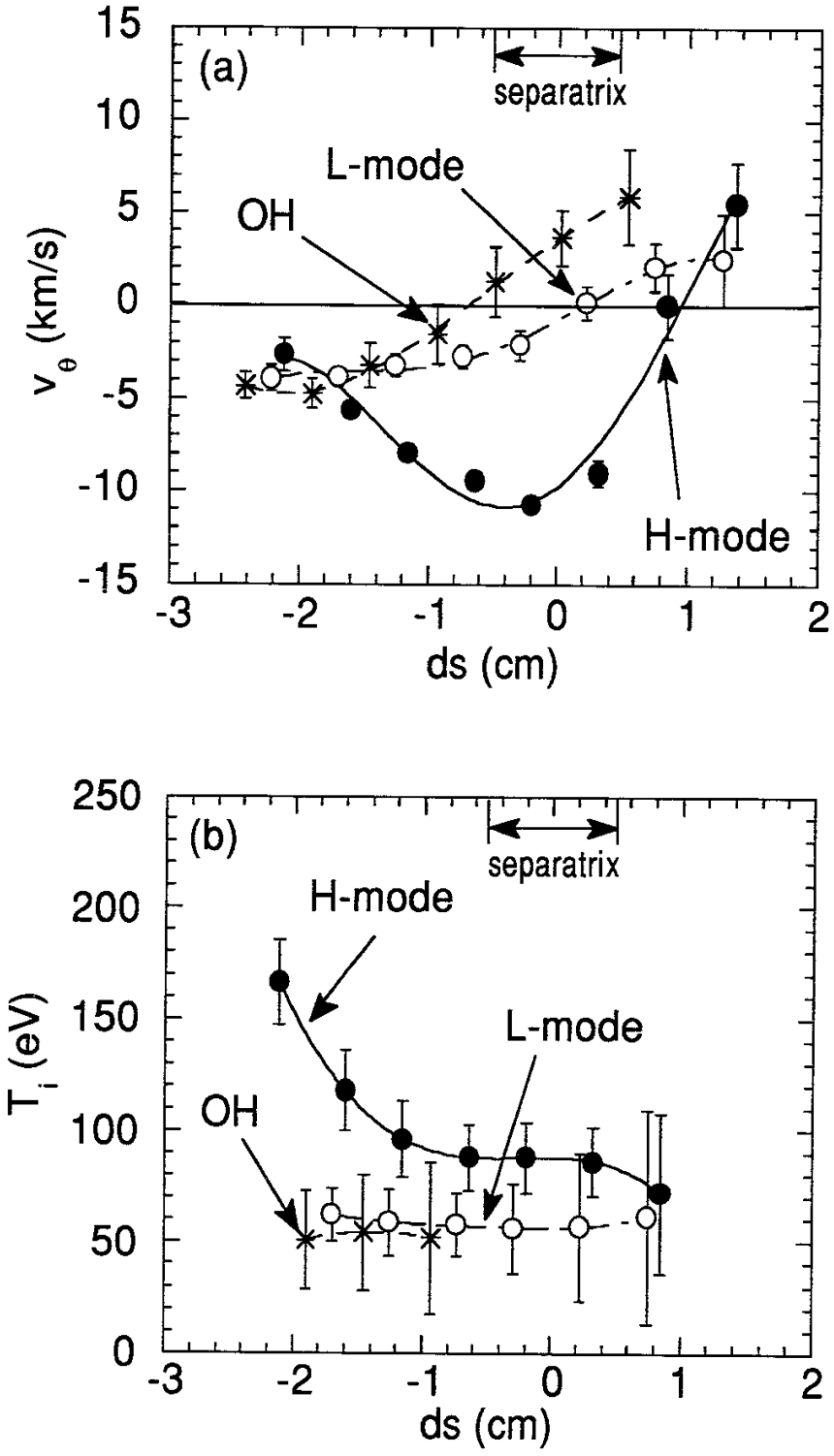
(a)
separatrix
L-mode
OH
H-mode
v_θ (km/s)
ds (cm)
(b)
separatrix
H-mode
L-mode
OH
T_i (eV)
ds (cm)

Figure 4

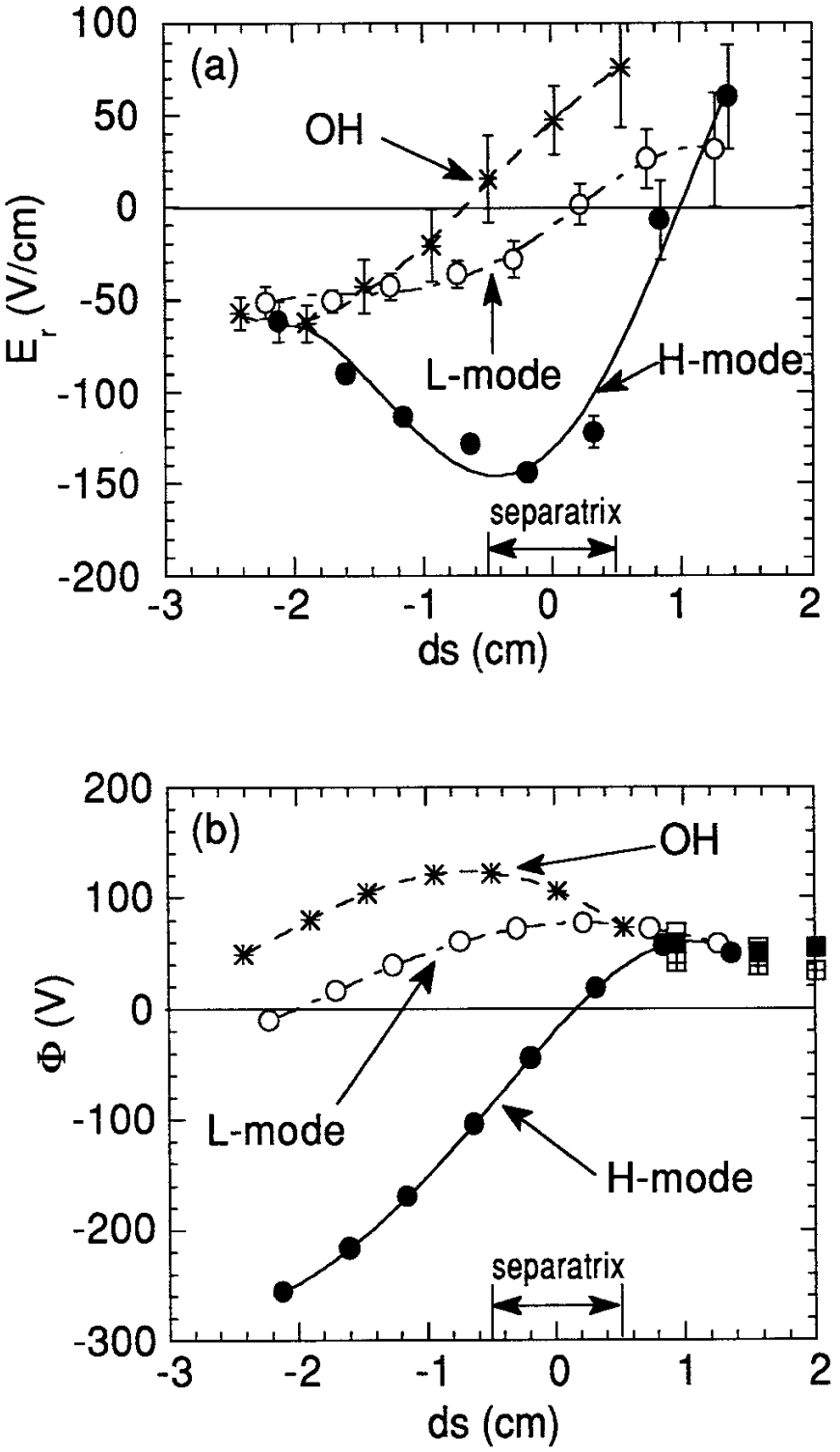
(a)
OH
L-mode
H-mode
separatrix
E_r (V/cm)
ds (cm)
100
50
0
-50
-100
-150
-200
-3
-2
-1
0
1
2
(b)
OH
L-mode
H-mode
separatrix
Φ (V)
ds (cm)
200
100
0
-100
-200
-300

Figure 5

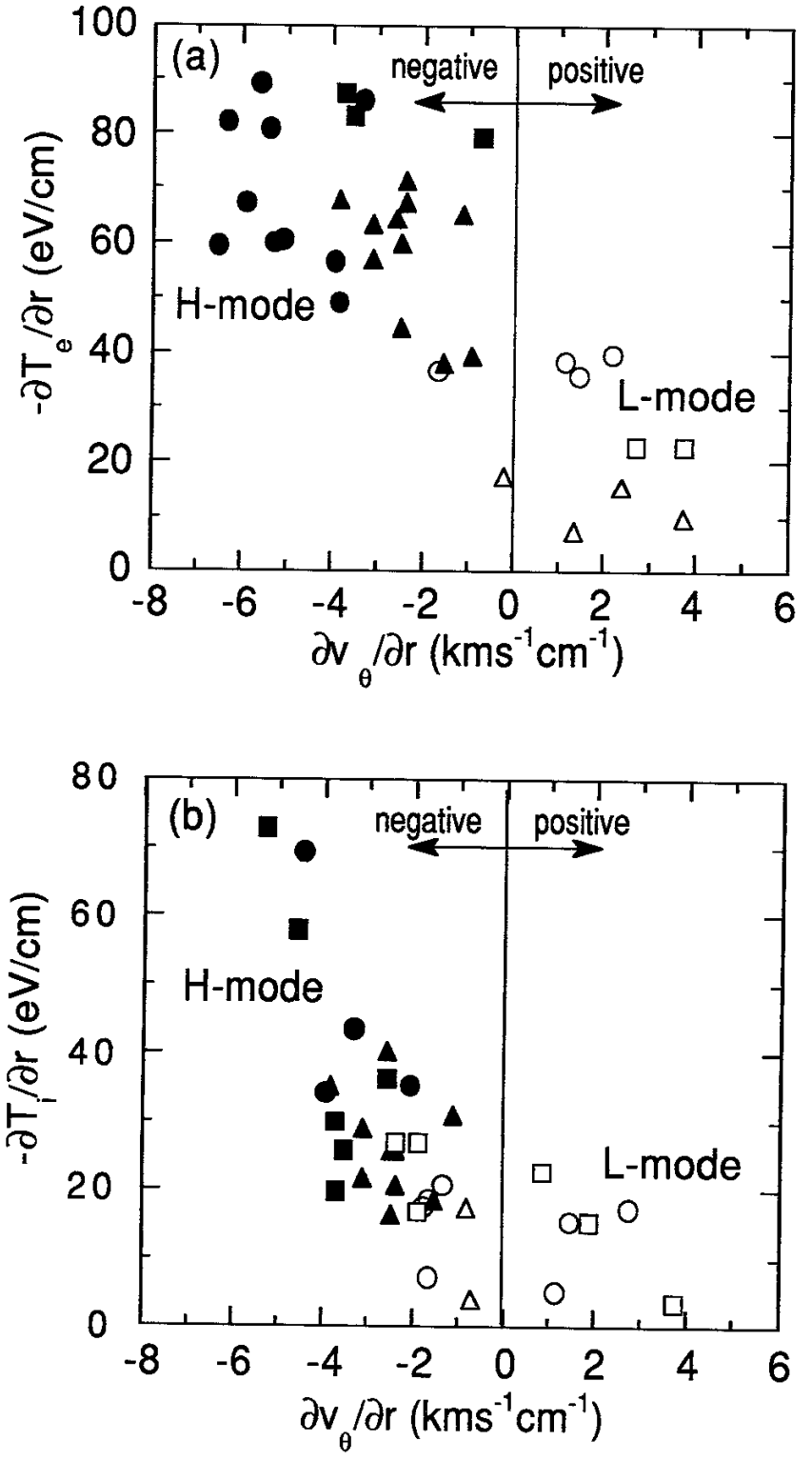
(a)
negative
positive
H-mode
L-mode
-∂T_e/∂r (eV/cm)
∂v_θ/∂r (kms^-1cm^-1)
100
80
60
40
20
0
-8
-6
-4
-2
0
2
4
6
(b)
negative
positive
H-mode
L-mode
-∂T_i/∂r (eV/cm)
∂v_θ/∂r (kms^-1cm^-1)
80
60
40
20
0
-8
-6
-4
-2
0
2
4
6

Figure 6

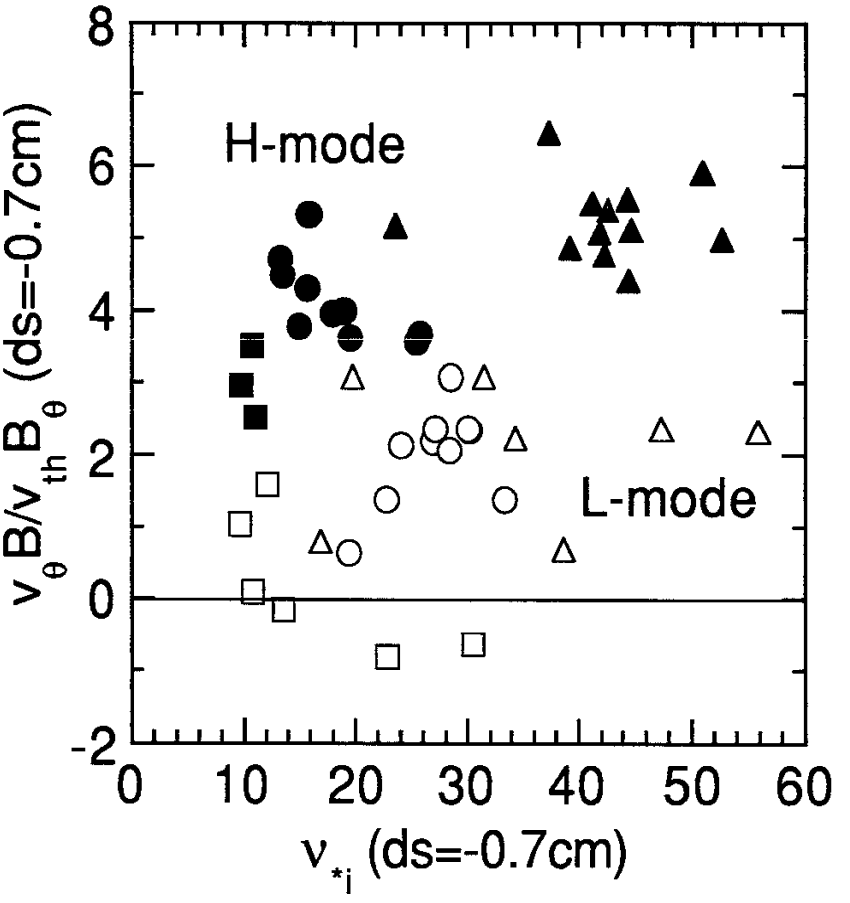
H-mode
L-mode
$\nu_\theta B/\nu_{th} B_\theta$ (ds=-0.7cm)
ν_{*i} (ds=-0.7cm)
8
6
4
2
0
-2
0
10
20
30
40
50
60

Figure 7

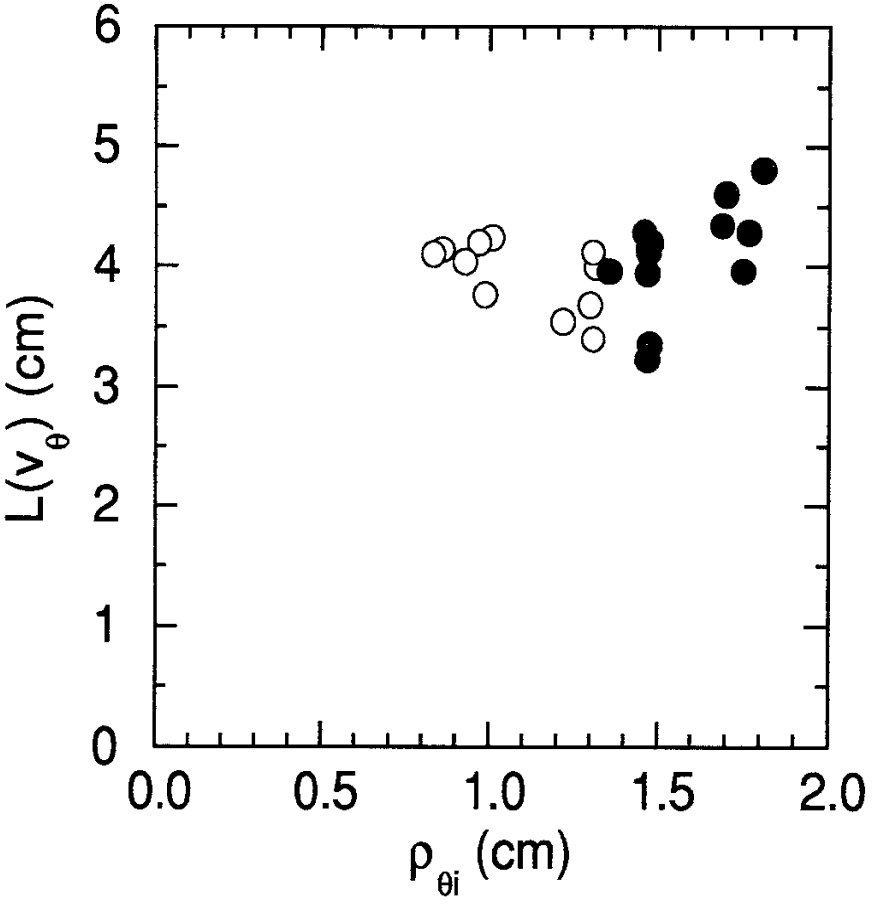

Figure 8

Recent Issues of NIFS Series

NIFS-65 A.Fukuyama, S.-I.Itoh and K. Itoh,*A Consistency Analysis on the Tokamak Reactor Plasmas;* Dec. 1990

NIFS-66 K.Itoh, H. Sanuki, S.-I. Itoh and K. Tani,*Effect of Radial Electric Field on α-Particle Loss in Tokamaks;* Dec. 1990

NIFS-67 K.Sato,and F.Miyawaki,*Effects of a Nonuniform Open Magnetic Field on the Plasma Presheath*; Jan.1991

NIFS-68 K.Itoh and S.-I.Itoh,*On Relation between Local Transport Coefficient and Global Confinement Scaling Law;* Jan. 1991

NIFS-69 T.Kato, K.Masai, T.Fujimoto,F.Koike, E.Källne, E.S.Marmar and J.E.Rice,*He-like Spectra Through Charge Exchange Processes in Tokamak Plasmas;* Jan.1991

NIFS-70 K. Ida, H. Yamada, H. Iguchi, K. Itoh and CHS Group, *Observation of Parallel Viscosity in the CHS Heliotron/Torsatron* ; Jan.1991

NIFS-71 H. Kaneko, *Spectral Analysis of the Heliotron Field with the Toroidal Harmonic Function in a Study of the Structure of Built-in Divertor* ; Jan. 1991

NIFS-72 S. -I. Itoh, H. Sanuki and K. Itoh, *Effect of Electric Field Inhomogeneities on Drift Wave Instabilities and Anomalous Transport* ; Jan. 1991

NIFS-73 Y.Nomura, Yoshi.H.Ichikawa and W.Horton, *Stabilities of Regular Motion in the Relativistic Standard Map*; Feb. 1991

NIFS-74 T.Yamagishi, *Electrostatic Drift Mode in Toroidal Plasma with Minority Energetic Particles,* Feb. 1991

NIFS-75 T.Yamagishi, *Effect of Energetic Particle Distribution on Bounce Resonance Excitation of the Ideal Ballooning Mode*, Feb. 1991

NIFS-76 T.Hayashi, A.Tadei, N.Ohyabu and T.Sato, *Suppression of Magnetic Surface Breading by Simple Extra Coils in Finite Beta Equilibrium of Helical System;* Feb. 1991

NIFS-77 N. Ohyabu, *High Temperature Divertor Plasma Operation*; Feb. 1991

NIFS-78 K.Kusano, T. Tamano and T. Sato, *Simulation Study of Toroidal Phase-Locking Mechanism in Reversed-Field Pinch Plasma*; Feb. 1991

NIFS-79 K. Nagasaki, K. Itoh and S. -I. Itoh, *Model of Divertor Biasing and Control of Scrape-off Layer and Divertor Plasmas*; Feb. 1991

NIFS-80 K. Nagasaki and K. Itoh, *Decay Process of a Magnetic Island by Forced Reconnection*; Mar. 1991

NIFS-81 K. Takahata, N. Yanagi, T. Mito, J. Yamamoto, O.Motojima and LHDDesign Group, K. Nakamoto, S. Mizukami, K. Kitamura, Y. Wachi, H. Shinohara, K. Yamamoto, M. Shibui, T. Uchida and K. Nakayama, *Design and Fabrication of Forced-Flow Coils as R&D Program for Large Helical Device*; Mar. 1991

NIFS-82 T. Aoki and T. Yabe, *Multi-dimensional Cubic Interpolation for ICF Hydrodynamics Simulation*; Apr. 1991

NIFS-83 K. Ida, S.-I. Itoh, K. Itoh, S. Hidekuma, Y. Miura, H. Kawashima, M. Mori, T. Matsuda, N. Suzuki, H. Tamai, T.Yamauchi and JFT-2M Group, *Density Peaking in the JFT-2M Tokamak Plasma with Counter Neutral Beam Injection* ; May 1991

NIFS-84 A. Iiyoshi, *Development of the Stellarator/Heliotron Research*; May 1991

NIFS-85 Y. Okabe, M. Sasao, H. Yamaoka, M. Wada and J. Fujita, *Dependence of Au^- Production upon the Target Work Function in a Plasma-Sputter-Type Negative Ion Source;* May 1991

NIFS-86 N. Nakajima and M. Okamoto, *Geometrical Effects of the Magnetic Field on the Neoclassical Flow, Current and Rotation in General Toroidal Systems*; May 1991

NIFS-87 S. -I. Itoh, K. Itoh, A. Fukuyama, Y. Miura and JFT-2M Group, *ELMy-H mode as Limit Cycle and Chaotic Oscillations in Tokamak Plasmas;* May 1991

NIFS-88 N.Matsunami and K.Kitoh, *High Resolution Spectroscopy of H^+ Energy Loss in Thin Carbon Film;* May 1991

NIFS-89 H. Sugama, N. Nakajima and M.Wakatani, *Nonlinear Behavior of Multiple-Helicity Resistive Interchange Modes near Marginally Stable States;* May 1991

NIFS-90 H. Hojo and T.Hatori, *Radial Transport Induced by Rotating RF Fields and Breakdown of Intrinsic Ambipolarity in a Magnetic Mirror*; May 1991

NIFS-91 M. Tanaka, S. Murakami, H. Takamaru and T.Sato, *Macroscale Implicit, Electromagnetic Particle Simulation of Inhomogeneous and Magnetized Plasmas in Multi-Dimensions;* May 1991

NIFS-92 S. - I. Itoh, *H-mode Physics, -Experimental Observations and Model Theories-, Lecture Notes, Spring College on Plasma Physics, May 27 - June 21 1991 at International Centre for Theoretical Physics (IAEA UNESCO) Trieste, Italy ;* Jun. 1991

NIFS-93 Y. Miura, K. Itoh, S. - I. Itoh, T. Takizuka, H. Tamai, T. Matsuda, N. Suzuki, M. Mori, H. Maeda and O. Kardaun, *Geometric Dependence of the Scaling Law on the Energy Confinement Time in H-mode Discharges;* Jun. 1991

NIFS-94 H. Sanuki, K. Itoh, K. Ida and S. - I. Itoh, *On Radial Electric Field Structure in CHS Torsatron / Heliotron;* Jun. 1991

NIFS-95 K. Itoh, H. Sanuki and S. - I. Itoh, *Influence of Fast Ion Loss on Radial Electric Field in Wendelstein VII-A Stellarator;* Jun. 1991

NIFS-96 S. - I. Itoh, K. Itoh, A. Fukuyama, *ELMy-H mode as Limit Cycle and Chaotic Oscillations in Tokamak Plasmas;* Jun. 1991

NIFS-97 K. Itoh, S. - I. Itoh, H. Sanuki, A. Fukuyama, *An H-mode-Like Bifurcation in Core Plasma of Stellarators;* Jun. 1991

NIFS-98 H. Hojo, T. Watanabe, M. Inutake, M. Ichimura and S. Miyoshi, *Axial Pressure Profile Effects on Flute Interchange Stability in the Tandem Mirror GAMMA 10;* Jun. 1991

NIFS-99 A. Usadi, A. Kageyama, K. Watanabe and T. Sato, *A Global Simulation of the Magnetosphere with a Long Tail : Southward and Northward IMF;* Jun. 1991

NIFS-100 H. Hojo, T. Ogawa and M. Kono, *Fluid Description of Ponderomotive Force Compatible with the Kinetic One in a Warm Plasma* ; July 1991

NIFS-101 H. Momota, A. Ishida, Y. Kohzaki, G. H. Miley, S. Ohi, M. Ohnishi K. Yoshikawa, K. Sato, L. C. Steinhauer, Y. Tomita and M. Tuszewski *Conceptual Design of D-^{3}He FRC Reactor "ARTEMIS"* ; July 1991

NIFS-102 N. Nakajima and M. Okamoto, *Rotations of Bulk Ions and Impurities in Non-Axisymmetric Toroidal Systems* ; July 1991

NIFS-103 A. J. Lichtenberg, K. Itoh, S. - I. Itoh and A. Fukuyama, *The Role of Stochasticity in Sawtooth Oscillation* ; Aug. 1991

NIFS-104 K. Yamazaki and T. Amano, *Plasma Transport Simulation Modeling for Helical Confinement Systems;* Aug. 1991

NIFS-105 T. Sato, T. Hayashi, K. Watanabe, R. Horiuchi, M. Tanaka, N. Sawairi and K. Kusano, *Role of Compressibility on Driven Magnetic Reconnection ;* Aug. 1991

NIFS-106 Qian Wen - Jia, Duan Yun - Bo, Wang Rong - Long and H. Narumi, *Electron Impact Excitation of Positive Ions - Partial Wave Approach in Coulomb - Eikonal Approximation* ; Sep. 1991

NIFS-107 S. Murakami and T. Sato, *Macroscale Particle Simulation of Externally Driven Magnetic Reconnection;* Sep. 1991

NIFS-108 Y. Ogawa, T. Amano, N. Nakajima, Y. Ohyabu, K. Yamazaki, S. P. Hirshman, W. I. van Rij and K. C. Shaing, *Neoclassical Transport Analysis in the Banana Regime on Large Helical Device (LHD) with the DKES Code;* Sep. 1991

NIFS-109 Y. Kondoh, *Thought Analysis on Relaxation and General Principle to Find Relaxed State;* Sep. 1991

NIFS-110 H. Yamada, K. Ida, H. Iguchi, K. Hanatani, S. Morita, O. Kaneko, H. C. Howe, S. P. Hirshman, D. K. Lee, H. Arimoto, M. Hosokawa, H. Idei, S. Kubo, K. Matsuoka, K. Nishimura, S. Okamura, Y. Takeiri, Y. Takita and C. Takahashi, *Shafranov Shift in Low-Aspect-Ratio Heliotron / Torsatron CHS* ; Sep 1991

NIFS-111 R. Horiuchi, M. Uchida and T. Sato, *Simulation Study of Stepwise Relaxation in a Spheromak Plasma ;* Oct. 1991

NIFS-112 M. Sasao, Y. Okabe, A. Fujisawa, H. Iguchi, J. Fujita, H. Yamaoka and M. Wada, *Development of Negative Heavy Ion Sources for Plasma Potential Measurement* ; Oct. 1991

NIFS-113 S. Kawata and H. Nakashima, *Tritium Content of a DT Pellet in Inertial Confinement Fusion* ; Oct. 1991

NIFS-114 M. Okamoto, N. Nakajima and H. Sugama, *Plasma Parameter Estimations for the Large Helical Device Based on the Gyro-Reduced Bohm Scaling* ; Oct. 1991

NIFS-115 Y. Okabe, *Study of Au^- Production in a Plasma-Sputter Type Negative Ion Source* ; Oct. 1991

NIFS-116 M. Sakamoto, K. N. Sato, Y. Ogawa, K. Kawahata, S. Hirokura, S. Okajima, K. Adati, Y. Hamada, S. Hidekuma, K. Ida, Y. Kawasumi, M. Kojima, K. Masai, S. Morita, H. Takahashi, Y. Taniguchi, K. Toi and T. Tsuzuki, *Fast Cooling Phenomena with Ice Pellet Injection in the JIPP T-IIU Tokamak;* Oct. 1991

NIFS-117 K. Itoh, H. Sanuki and S. -I. Itoh, *Fast Ion Loss and Radial Electric Field in Wendelstein VII-Λ Stellarator*; Oct. 1991

NIFS-118 Y. Kondoh and Y. Hosaka, *Kernel Optimum Nearly-analytical Discretization (KOND) Method Applied to Parabolic Equations <<KOND-P Scheme>>;* Nov. 1991

NIFS-119 T. Yabe and T. Ishikawa, *Two- and Three-Dimensional Simulation Code for Radiation-Hydrodynamics in ICF*; Nov. 1991

NIFS-120 S. Kawata, M. Shiromoto and T. Teramoto, *Density-Carrying Particle Method for Fluid* ; Nov. 1991

NIFS-121 T. Ishikawa, P. Y. Wang, K. Wakui and T. Yabe, *A Method for the High-speed Generation of Random Numbers with Arbitrary Distributions;* Nov. 1991

NIFS-122 K. Yamazaki, H. Kaneko, Y. Taniguchi, O. Motojima and LHD Design Group, *Status of LHD Control System Design* ; Dec. 1991

NIFS-123 Y. Kondoh, *Relaxed State of Energy in Incompressible Fluid and Incompressible MHD Fluid* ; Dec. 1991